

Original Article

Numerical simulation of heat transfer over a torus rotating about its centerline

Jakgrit Sompong^{1*} and Pairin Suwannasri²¹ Department of Mathematics, Faculty of Science,
Naresuan University, Mueang, Phitsanulok, 65000 Thailand² Department of Mathematics Statistics and Computer, Faculty of Science,
Ubon Ratchathani University, Warin Chamrap, Ubon Ratchathani, 34190 Thailand

Received: 8 November 2017; Revised: 28 February 2018; Accepted: 27 April 2018

Abstract

The heat transfer characteristics of axisymmetric flow past a rotating torus in viscous incompressible fluid have been investigated numerically. The torus surface rotates about its centerline with constant velocity. The governing equations in a toroidal coordinate system are solved by using a finite difference method for ranges of parameters: Reynolds number $20 \leq Re \leq 40$; Prandtl number $0.7 \leq Pr \leq 100$; rotational speed $0 \leq \alpha \leq 1.9$; and fixed aspect ratio $Ar = 2$. The heat transfer characteristics are presented in terms of the isotherm patterns, local Nusselt numbers, and average Nusselt numbers. Variation of the local Nusselt number on the torus surface shows the effect of the Prandtl number and rotational speed on heat transfer from a torus in the flow regime. Torus rotation is an efficient Nusselt number reduction or torus surface temperature enhancement technique.

Keywords: heat transfer, rotating torus, viscous incompressible fluid, axisymmetric flow

1. Introduction

Heat and fluid flow past bluff bodies have been extensively studied by many researchers for a long time. With their simple geometrical shape and wide variety of practical applications examples that were studied are circular cylinder (Bharti, Chhabra, & Eswaran, 2006, 2007; Juncu, 2007; Khan, Culham, & Yovanovich, 2005; Lange, Durst, & Breuer, 1998; Moshkin & Sompong, 2010; Soares, Ferreira, & Chhabra, 2005; Sungnul & Moshkin, 2006), sphere (Dennis, Walker, & Hudson, 1973; Dhole, Chhabra, & Eswaran, 2006; Feng & Michaelides, 2000), and torus or ring (Moshkin & Suwannasri, 2010; Moshkin, Sompong, & Suwannasri, 2013; Sheard, Hourigan, & Thompson, 2003; Suwannasri, 2016).

The flow past a torus is a basic concept that can be extensively applied to many problems such as bio-fluid mechanics for DNA polymers, properties of flow with micelles, and the drag and heat transfer performance for helical heating tubes. The present work concerns the heat transfer over a torus rotating about its centerline. The geometry of a torus (Figure 1) can be characterized by its aspect ratio $Ar = b/a$, which is the ratio of the center-line diameter of the torus $2b$ to the cross-section diameter of the torus $2a$. When $Ar = 0$, the torus becomes a sphere. On the other hand, it becomes a single cylinder as $Ar \rightarrow \infty$ (Sheard *et al.*, 2003).

The problem of flow past a rotating torus has not been investigated widely in the literature. Under the influence of rotation, the uniform flow across a torus is useful for flow control, lift enhancement, and reduction of drag force and heat transfer. For flow across a rotating torus, the results not only depend on the Reynolds number (Re), Prandtl number (Pr), and aspect ratio (Ar) but also depend on the rotational velocity (α). The rotational velocity represents the torus

*Corresponding author
Email address: jakgrits@nu.ac.th

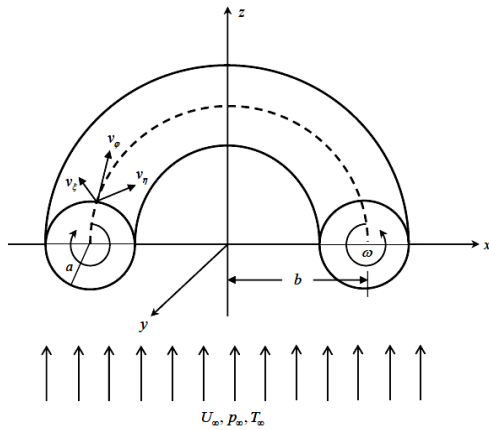


Figure 1. Sketch of the geometry of the torus.

surface tangential velocity in terms of free stream flow velocity.

The preliminary results of flow and heat transfer over a stationary torus placed in a uniform flow was reported in our earlier work (Moshkin *et al.*, 2013) for ranges of Reynolds numbers $20 \leq Re \leq 40$, Prandtl numbers $0.7 \leq Pr \leq 100$, and aspect ratios $1.4 \leq Ar \leq 20$. In this paper, the objective is to extend the heat transfer study from flow past a stationary torus to flow past a torus rotating about its centerline for some ranges of Re , extended Prandtl numbers in the ranges of $0.7 \leq Pr \leq 100$, and a fixed aspect ratio of $Ar = 2$. The mathematical formulation for the problem is described in Section 2. The problem is recast in terms of the toroidal coordinate system. Section 3 presents the numerical algorithm based on the projection method for solving the Navier-Stokes equations. The various numerical results are reported and discussed in the final part.

2. Mathematical Formulation for the Problem

The physical system that we considered is shown in Figure 1 which consists of a torus with meridional cross-sectional radius a , torus radius b , and surface S_b , where it is placed axisymmetrically in a uniform stream (from bottom to top) in which the flow has constant properties of velocity U_∞ , pressure p_∞ , and temperature T_∞ . The fluid is viscous and incompressible with constant properties of density ρ and viscosity μ .

The best suited coordinate system for the problem under consideration is the toroidal coordinate system. In terms of the toroidal coordinates and the assumption of axisymmetry, the governing Navier-Stokes equations in dimensionless form are given by

Momentum equations:

$$\begin{aligned} \frac{\partial v_\xi}{\partial t} + \frac{1}{h} \left(v_\xi \frac{\partial v_\xi}{\partial \xi} + v_\eta \frac{\partial v_\xi}{\partial \eta} \right) + \frac{1}{c} (v_\eta^2 \sin \xi - v_\xi v_\eta \sinh \eta) = -\frac{1}{h} \frac{\partial p}{\partial \xi} + \frac{2}{Re} \left[\frac{1}{h^2} \left(\frac{\partial^2 v_\xi}{\partial \xi^2} + \frac{\partial^2 v_\xi}{\partial \eta^2} \right) \right. \\ \left. - \frac{1}{ch} \left(\sin \xi \frac{\partial v_\xi}{\partial \xi} + 2 \sinh \eta \frac{\partial v_\xi}{\partial \xi} - 2 \sin \xi \frac{\partial v_\eta}{\partial \eta} \right) + \left(\frac{\coth \eta}{h^2} - \frac{1}{ch} \sinh \eta \right) \frac{\partial v_\xi}{\partial \eta} + \frac{1}{c^2} (\cosh \eta \cos \xi - 1) v_\xi \right. \\ \left. + \left(\frac{1}{ch} \cosh \eta - \frac{2}{c^2} (\sin^2 \xi + \sinh^2 \eta) \right) v_\xi + \left(\frac{\sin \xi}{c^2 \sinh \eta} ((2 - 2 \cosh \eta \cos \xi) + \sinh^2 \eta) \right) v_\eta \right] \end{aligned} \tag{1}$$

$$\begin{aligned} \frac{\partial v_\eta}{\partial t} + \frac{1}{h} \left(v_\xi \frac{\partial v_\eta}{\partial \xi} + v_\eta \frac{\partial v_\eta}{\partial \eta} \right) + \frac{1}{c} (v_\xi^2 \sinh \eta - v_\xi v_\eta \sin \xi) = -\frac{1}{h} \frac{\partial p}{\partial \eta} + \frac{2}{Re} \left[\frac{1}{h^2} \left(\frac{\partial^2 v_\eta}{\partial \xi^2} + \frac{\partial^2 v_\eta}{\partial \eta^2} \right) \right. \\ \left. - \frac{1}{ch} \left(\sin \xi \frac{\partial v_\eta}{\partial \xi} - 2 \sinh \eta \frac{\partial v_\xi}{\partial \xi} + 2 \sin \xi \frac{\partial v_\xi}{\partial \eta} \right) + \left(\frac{\coth \eta}{h^2} - \frac{\sinh \eta}{ch} \right) \frac{\partial v_\eta}{\partial \eta} - \frac{\sin \xi \sinh \eta}{c^2} v_\xi \right. \\ \left. + \left(\frac{\cosh \eta}{ch} - \frac{2}{c^2} (\sin^2 \xi + \sinh^2 \eta) \right) v_\eta + \frac{1}{c^2} \left(\sin^2 \xi + (\cosh \eta \cos \xi - 1) + \frac{(1 - \cosh \eta \cos \xi)^2}{\sinh^2 \eta} \right) v_\eta \right] \end{aligned} \tag{2}$$

Continuity equation:

$$\frac{1}{h} \left(\frac{\partial v_\xi}{\partial \xi} + \frac{\partial v_\eta}{\partial \eta} \right) - \frac{2h \sin \xi}{c} v_\xi + \left(\coth \eta - \frac{2h \sinh \eta}{c} \right) v_\eta = 0, \tag{3}$$

Energy equation:

$$\frac{\partial T}{\partial t} + \frac{1}{h} \left(v_\xi \frac{\partial T}{\partial \xi} + v_\eta \frac{\partial T}{\partial \eta} \right) = \frac{2}{Re Pr} \frac{1}{h^3 \sinh \eta} \left\{ \frac{\partial}{\partial \xi} \left(h \sinh \eta \frac{\partial T}{\partial \xi} \right) + \frac{\partial}{\partial \eta} \left(h \sinh \eta \frac{\partial T}{\partial \eta} \right) \right\} \quad (4)$$

where ρ is the pressure, v_ξ , and v_η are the velocity components in ξ and η directions, respectively, and $h = c / (\cosh \eta - \cos \xi)$. The governing equations are made dimensionless using the following scaling variables: radius of a cross-section of torus a for length variables, U_∞ for velocities, a / U_∞ for time, and ρU_∞^2 for pressure. The temperature is non-dimensionalized using $(T - T_\infty) / (T_w - T_\infty)$. Here Re denotes the Reynolds number defined by $Re = \frac{2U_\infty a}{\nu}$, the Prandtl number is given by $Pr = \frac{c_p \mu}{\kappa}$ where μ the viscosity of the fluid, $\nu = \mu / \rho$ is the kinematic viscosity, c_p is the heat capacity, and κ is the thermal conductivity.

The boundary conditions based on the problem are as follows:

- Torus surface: We use the no-slip, impermeability and constant temperature conditions on the right computational boundary of Figure 2.

$$v_\xi = \alpha, \quad v_\eta = 0, \quad \text{and} \quad T = 1, \quad \xi \in (0, 2\pi], \quad \eta = \eta_0. \quad (5)$$

where $\alpha = (a\omega) / U_\infty$ is the nondimensional rotational velocity at the surface.

- Periodicity conditions: We use the periodic conditions for all variables on the bottom and top boundaries of Figure 2.

$$\begin{aligned} v_\xi(\xi, \eta) &= v_\xi(\xi + 2\pi, \eta), & v_\eta(\xi, \eta) &= v_\eta(\xi + 2\pi, \eta), \\ p(\xi, \eta) &= p(\xi + 2\pi, \eta), & T(\xi, \eta) &= T(\xi + 2\pi, \eta). \end{aligned} \quad (6)$$

- At infinity: We use the uniform flow condition at the far-field boundary which is the boundary of domains Ω_1 and Ω_2 in Figure 2.

$$\vec{v} = (v_r, v_z) = (0, 1), \quad p = \frac{P_\infty}{\rho U_\infty^2}, \quad T = 0 \quad \text{as} \quad r^2 + z^2 \rightarrow \infty. \quad (7)$$

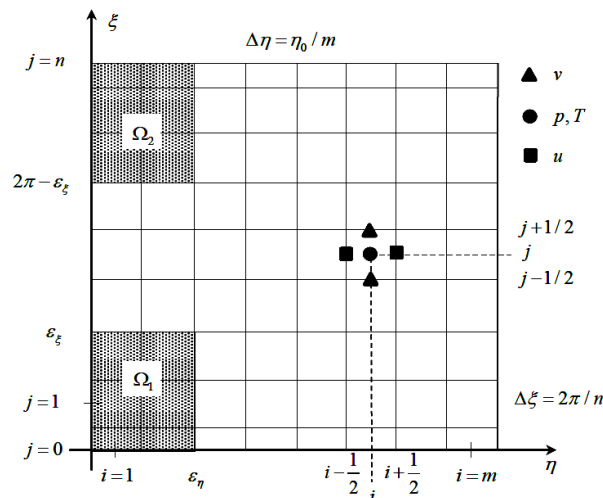


Figure 2. Staggered arrangement of u , v , p , and T in the computational domain.

Here, v_r and v_z are the components of the velocity vector in the cylindrical coordinate system with

$$\begin{aligned}
 v_\xi &= \left(-\frac{h}{a} \sinh \eta \sin \xi\right) v_r + \left(\frac{h}{a} (\cosh \eta \cos \xi - 1)\right) v_z, \\
 v_\eta &= \left(-\frac{h}{a} (\cosh \eta \cos \xi - 1)\right) v_r - \left(\frac{h}{a} \sinh \eta \sin \xi\right) v_z.
 \end{aligned}
 \tag{8}$$

- Axis of symmetry ($r=0$): The velocity components, pressure, and temperature on the left computational domain boundary are satisfied under the following conditions:

$$\frac{\partial v_\xi}{\partial \eta} = 0, \quad v_\eta = 0, \quad \frac{\partial p}{\partial \eta} = 0 \quad \text{and} \quad \frac{\partial T}{\partial \eta} = 0.
 \tag{9}$$

The two most important hydrodynamic characteristics of the flow around the body are the net force and angular momentum. The net force is decomposed into two components F_L and F_D that are perpendicular and parallel to the flow direction, respectively. The net torque and F_L are equal to zero due to the symmetry of the flow. The drag coefficient is defined as $C_D = \frac{F_D}{0.5 \rho A_{frontal} U_\infty^2}$, where ρ and $A_{frontal}$ are the fluid density and the projected frontal area of the body, respectively. The drag coefficient is comprised of a pressure drag coefficient and a viscous drag coefficient, i.e. $C_D = C_{D_p} + C_{D_f}$. They are defined as

$$C_{D_p} = -\frac{\sinh^2 \eta_0}{b} \int_0^{2\pi} p \frac{\sin \xi}{(\cosh \eta_0 - \cos \xi)} h^2 d\xi, \quad C_{D_f} = -\frac{\sinh^2 \eta_0}{b} \int_0^{2\pi} \frac{2\omega (\cosh \eta_0 - 1)}{Re (\cosh \eta_0 - \cos \xi)} h d\xi.
 \tag{10}$$

The vorticity ω is defined by the following equation:

$$\omega = \frac{1}{h^3 \sinh \eta_0} \left(\frac{\partial}{\partial \xi} (h v_\eta) - \frac{\partial}{\partial \eta} (h v_\xi) \right).
 \tag{11}$$

The important parameter of interest in heat transfer problems is the heat transfer rate per unit area from the torus wall to the ambient fluid. The local Nusselt number in the toroidal coordinate system based on the diameter of the torus is defined as

$$Nu = -\left(\frac{\partial T}{\partial n}\right) = -\left(\frac{\cosh \eta - \cos \xi}{a}\right) \frac{\partial T}{\partial \eta}.
 \tag{12}$$

The average Nusselt number is calculated by averaging the local Nusselt number over the surface of the torus.

$$\overline{Nu} = -\frac{\sinh(\eta_0)}{2\pi ab} \int_0^{2\pi} h^2 Nu \, d\xi.
 \tag{13}$$

3. Numerical Methods of Solution

In the case of steady flow, time in equations (1), (2), and (4) can be considered as an artificial (iterative) parameter. A staggered placement of variables is used with velocity components $u = v_\eta$ located on the vertical sides of each cell and components $v = v_\xi$ on the horizontal sides of each cell. Pressure p and temperature T are represented at the center of each cell.

A two-step time-split projection method is utilized to advance the flow field. First, the velocity components are advanced from time level “ n ” to an intermediate level “*” by solving (1) and (2) explicitly without the pressure term. In the advection-diffusion step, the spatial derivatives are approximated by the central finite differences. One side finite differences are utilized near boundaries due to the staggered arrangement of variables. Then, the Poisson equation for the pressure is solved fully implicitly by the method of stabilizing correction (Yanenko, 1971). The equation for pressure is derived using the mass conservation requirement for each computational cell. Once the pressure is updated, the final level is computed with a pressure-correction step. When the steady solution of Navier-Stokes equations (1)-(3) is computed, the iterative method of stabilizing correction is used to find the steady distribution of the temperature field given by equation (4).

Figure 2 shows the computational domain, the sketch of the grid, and the location of the unknowns. Far-field boundary conditions (7) are shifted on the boundary of domains Ω_1 and Ω_2 which are defined as

$$\begin{aligned}\Omega_1 &= \left\{ (\xi, \eta) \mid 0 \leq \xi \leq \varepsilon_\xi, 0 \leq \eta \leq \varepsilon_\eta \right\}, \\ \Omega_2 &= \left\{ (\xi, \eta) \mid 2\pi - \varepsilon_\xi \leq \xi \leq 2\pi, 0 \leq \eta \leq \varepsilon_\eta \right\},\end{aligned}\quad (14)$$

where, $\varepsilon_\eta = K\Delta_\eta$ and $\varepsilon_\xi = M\Delta_\xi$, K , and M are integer numbers, and Δ_η and Δ_ξ are the sizes of the computational cells in the η and ξ directions, respectively.

4. Results and Discussion

4.1 Validation of the results

The grid refinement test was carried out for two Reynolds numbers $Re = 20$ and 40 and three aspect ratios $Ar = 2, 3, \text{ and } 20$. Three grids with refinement factor $h_{coarse} / h_{fine} = 1.5$ were used. The grid convergence indices were estimated in the standard way with the factor 1.25 (Roache, 1994). To reach a numerical solution, the computations were advanced in time (artificial time) until the drag coefficient had reached a constant value. The main simulation was carried out with dimensionless time steps of 0.0001 that were chosen in agreement with stability requirements.

Little data are available in the literature to verify the accuracy of flow and heat transfer over a torus rotating about its centerline. We expected that the flow and heat transfer over a torus at large Ar would be similar to the flow and heat transfer over two circular cylinders with large gap between the cylinder surfaces (Moshkin *et al.*, 2013; Moshkin & Suwannasri, 2010). The average Nusselt number for $Ar = 20$, $Re = 20, 30, 40$, and $Pr = 0.7 - 10.0$ was compared with data from the literature for heat transfer around two circular cylinders with a large gap and single cylinder. The deviations between our numerical results and the values in the literature were within $\pm 5\%$. The Nusselt number distribution on the torus surface with $Re = 20, 40$, $Ar = 20$ and $Pr = 0.7 - 10.0$ was compared with Bharti (2007) for the local Nusselt number on the surface of a single cylinder. Our numerical results were good and in agreement with the work by Bharti. More details can be seen from Moshkin *et al.*, (2013).

In order to validate the computational code of flow around a rotating torus, we developed the numerical code for the flow past two rotating cylinders. The drag coefficients C_D for $Re = 20$, $Ar = 20$ and four different rotational speeds ($\alpha = 0, 0.5, 1.0$ and 2.0) were considered. The difference between our results and the results of Sungnul and Moshkin (2006) for two rotating cylinders as well as the results of Chung (2006) for the case of one rotating cylinder were in the range of 2% to 3% (Moshkin & Suwannasri, 2010).

The comparisons of our numerical results with the literature data allowed us to conclude that the numerical method and computer code were well suited and can be used to simulate the flow and convective heat transfer over a torus rotating about its centerline.

4.2 Temperature contours

Because of axial symmetry, we present the temperature patterns only in a cross section of the torus. The details of temperature contours in the vicinity of the torus are presented in Figure 3 for the case of $Re = 30$, $Ar = 2$, $\alpha = 0, 1, 1.5, 1.9$, and $Pr = 0.7, 10, 20$. This figure demonstrates the effect of both rotational speed and Prandtl number on the temperature field. For $\alpha = 0$, and $Pr \geq 10$, there are almost separate wake-types of downstream isotherm patterns (Figures 3: 1st-column, 2nd and 3rd-rows). As α increases, the isotherms near the torus incline more toward the hole corresponding to the rotational direction. When $\alpha \geq 1$, the vortex shedding at the hole side of a rigid torus does not occur but vortex shedding occurs only at the outside shear layers on the side of free stream which results in the single bluff-body wake pattern while the outer isotherms elongate

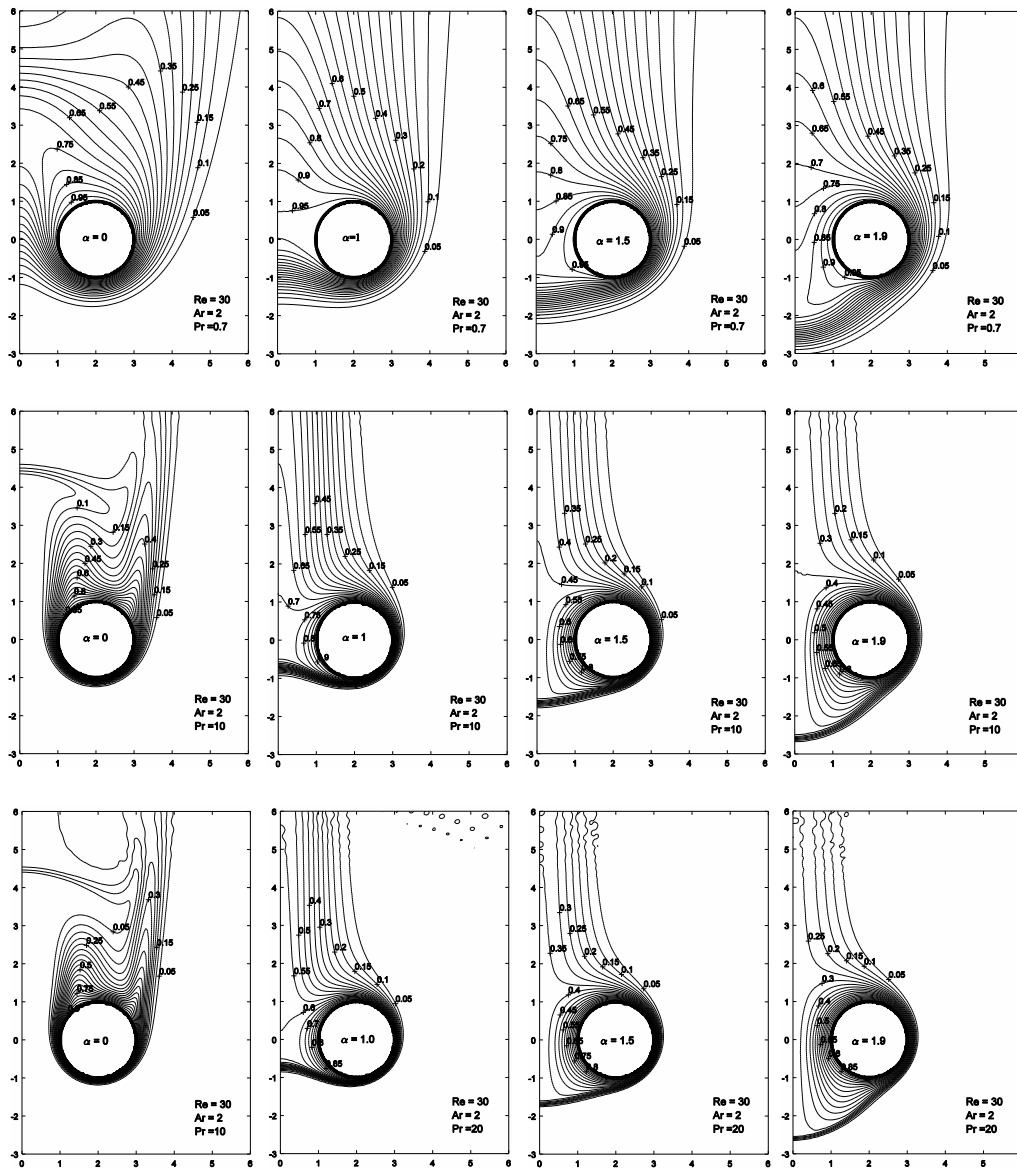


Figure 3. Temperature contours over the torus at 1st column: $\alpha = 0$, 2nd column: $\alpha = 1$, 3rd column: $\alpha = 1.5$, and 4th column: $\alpha = 1.9$, 1st-row: $Pr = 0.7$, 2nd row: $Pr = 10$ and 3rd row: $Pr = 20$ for Reynolds number $Re = 30$ and $Ar = 2$.

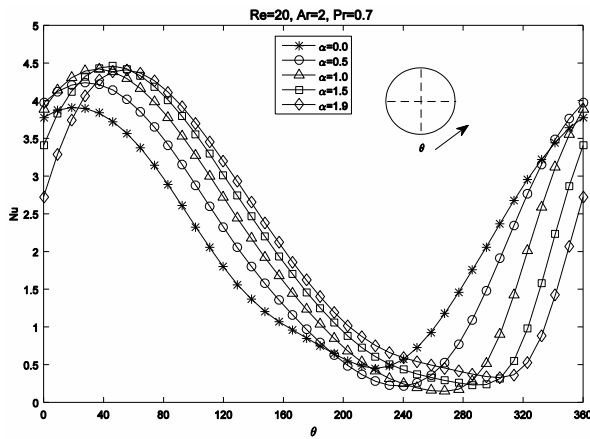
and decrease in the lateral width. Isotherm patterns depend on the Prandtl number. An increase in the Prandtl number at the same rotational speed leads to a narrow wake-shaped region of the temperature field and a decrease in the extension of the isothermal toward the downstream as shown in second, third, and fourth columns of Figure 3.

4.3 Local Nusselt number

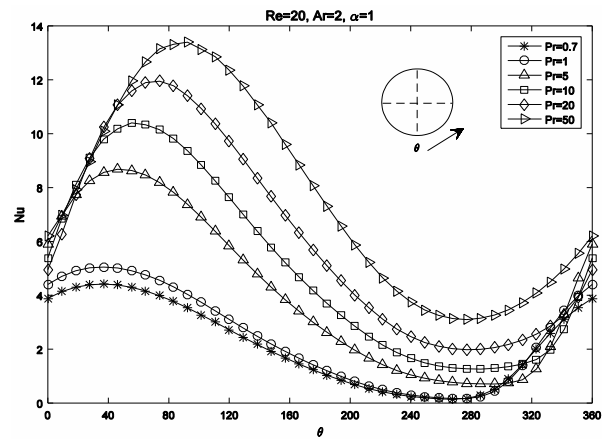
Variations of the local Nusselt number on the torus surface are shown in Figures 4 and 5. The circumferential direction θ varies from 0° to 360° and corresponds to the angular coordinate of the circular cross-section of the torus by

the meridional plane. Here, $\theta = 0^\circ$ represents the front stagnation point and $0^\circ \leq \theta \leq 180^\circ$ corresponds to the outer surface of the torus and $180^\circ \leq \theta \leq 360^\circ$ corresponds to the inner surface.

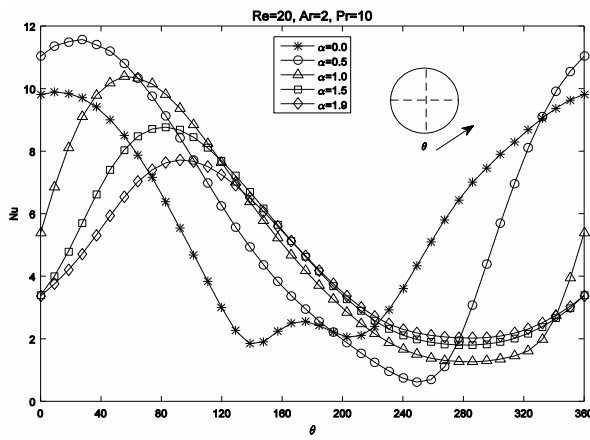
The local Nusselt numbers on the torus surface at $Re = 20$, $Ar = 2$ for different rotational speeds and three different Prandtl numbers are shown in Figure 4. In the case of $Pr = 0.7$, Figure 4a shows that an increase in rotational speed leads to a shift of the points of maximum and minimum values of the Nusselt number in the direction of rotation. Figure 4b and Figure 4c show that at $\alpha = 0$, the Nusselt number is almost symmetric about $\theta = 180^\circ$. The maximum/minimum



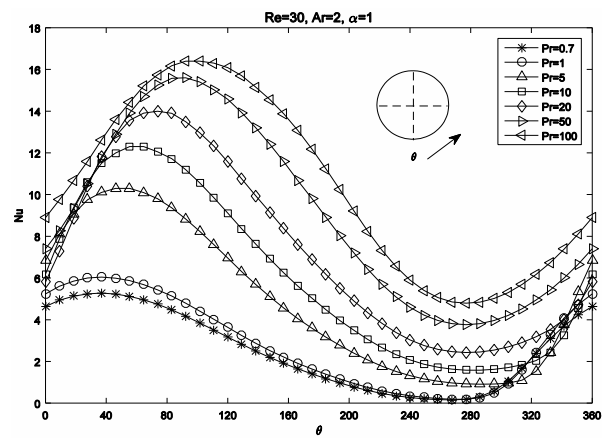
(a)



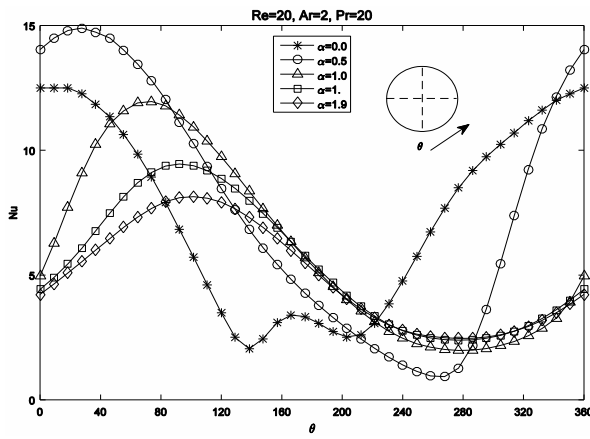
(a)



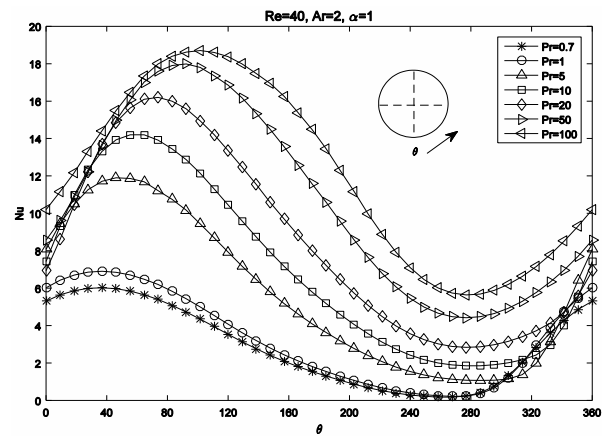
(b)



(b)



(c)



(c)

Figure 4. Local Nusselt number variations on the surface of the torus at $Re = 20$, $Ar = 2$ for different α , and (a) $Pr = 0.7$, (b) $Pr = 10$, and (c) $Pr = 20$.

Figure 5. Local Nusselt number variations on the surface of the torus at $Ar = 2$, $\alpha = 1$ for different Pr , and (a) $Re = 20$, (b) $Re = 30$, and (c) $Re = 40$.

values of the local Nusselt number decreases/increases when α increases from 0.5 to 1.9. For $\alpha \geq 1$ and at large Prandtl numbers ($Pr \geq 10$), the minimum values of Nu appear at the same position at $\theta = 280^\circ$. In Figure 4c, at $Pr = 20$, the

deviation of Nu becomes smaller on the inner side surface of the torus as $\alpha \geq 1.5$. This behavior is expected due to the no-slip condition.

Figure 5 shows the surface Nusselt number as a function of circumferential direction (θ) for various values of Prandtl number and three different Reynolds numbers ($Re = 20, 30,$ and 40) at $Ar = 2, \alpha = 1$. The numerical study shows that the Nusselt number always increases when the Prandtl number or Reynolds number or both increase. As the Prandtl number increases, the local Nusselt number increases up to the maximum value and after that it decreases to a minimum value at the rear part, $\theta = 280^\circ$ (see the second column in Figure 3).

4.4 Average Nusselt number

The effect of rotational speed (α) on the average Nusselt number (\overline{Nu}) at $Ar = 2, Re = 20, 40,$ and $Pr = 0.7 - 50$ is shown in Figure 6. At a fixed value of α , the value of \overline{Nu} increases monotonically as the Pr or Re or both increase. For all Pr considered in this study, the behavior of \overline{Nu} has the same decaying pattern with the

increasing α and also the reduction of local variation of Nusselt number with increasing α (Figure 4). The decreases in \overline{Nu} with increasing α can be explained on the basis that the region occupied by rotating fluid surrounding the torus enlarges as α increases, which prevents the main stream from penetrating the hole of the torus. Hence, the conduction mode is predominant to the heat transfer near the rotating torus.

5. Conclusions

The present work is a continuation of our previously published work (Moshkin *et al.*, 2013) for the flow and heat transfer around a stationary torus placed in uniform flow. The present work is a more detailed characteristic of heat transfer with a different rotational speed of the torus surface and Prandtl number. The numerical algorithm based on the projection method was developed to solve the Navier-Stokes equations in the toroidal coordinate system.

The present study numerically investigated the characteristics of 2D heat transfer past a torus rotating about its centerline for a various range of rotational speeds, $0 \leq \alpha \leq 1.9$, Prandtl numbers, $0.7 \leq Pr \leq 100$, Reynolds numbers, $20 \leq Re \leq 40$, at a small aspect ratio of the torus, $Ar = 2$. As α increases, the isotherms near the torus incline more toward the hole corresponding to the rotational direction. An increase in Pr generates a narrow wake-shaped region and a decrease in the extension of the isothermal toward the downstream. An increase in α leads to a shift in the points of maximum and minimum values of the local Nusselt number in the direction of rotation. The average Nusselt number was found to decrease as α increases and found to increase as Pr increases.

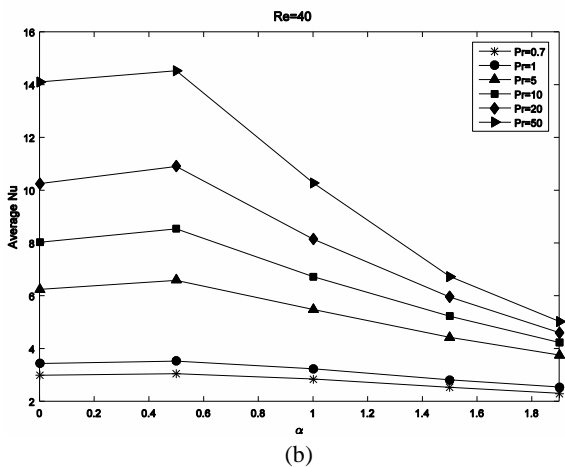
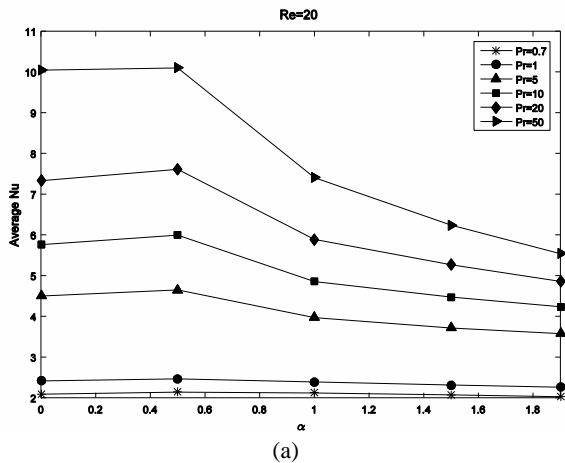


Figure 6. Average Nusselt number (\overline{Nu}) at $Ar = 2$ for different Pr and (a) $Re = 20$, and (b) $Re = 40$.

References

Bharti, R. P., Chhabra, R. P., & Eswaran, V. (2006). A numerical study of the steady forced convection heat transfer from an unconfined circular cylinder. *Heat Mass Transfer*, 43(7), 639-648.

Bharti, R. P., Chhabra R. P., & Eswaran, V. (2007). Steady forced convection heat transfer from a heated circular cylinder to power-law fluids. *International Journal of Heat and Mass Transfer*, 50(5-6), 977-990.

Chung, M. -H. (2006). Cartesian cut cell approach for simulating incompressible flows with rigid bodies of arbitrary shape. *Computers and Fluids*, 35(6), 607-623.

Dennis, S. C. R., Walker, J. D. A., & Hudson, J. D. (1973). Heat transfer from a sphere at low Reynolds numbers. *Journal of Fluid Mechanics*, 60(2), 273-283.

Dhole, S. D., Chhabra, R. P., & Eswaran, V. (2006). A numerical study on the forced convection heat transfer from an isothermal and isoflux sphere in the

- steady symmetric flow regime. *International Journal of Heat and Mass Transfer*, 49(5-6), 984-994.
- Feng, Z. -G., & Michaelides, E. E. (2000). A Numerical Study on the Transient Heat Transfer from a Sphere at High Reynolds and Peclet Numbers. *International Journal of Heat and Mass Transfer*, 43(2), 219-229.
- Juncu, G. (2007). A numerical study of momentum and forced convection heat transfer around two tandem circular cylinders at low Reynolds numbers. Part II: Forced convection heat transfer. *International Journal of Heat and Mass Transfer*, 50(19-20), 3799-3808.
- Khan, W. A., Culham, J. R., & Yovanovich, M. M. (2005). Fluid flow around and heat transfer from an infinite circular cylinder. *Journal of Heat Transfer*, 127(7), 785-790.
- Lange, C. F., Durst, F., & Breuer, M. (1998). Momentum and heat transfer from cylinders in laminar crossflow at $10-4 \leq Re \leq 200$. *International Journal of Heat and Mass Transfer*, 41(22), 3409-3430.
- Moshkin, N. P., & Sompong, J. (2010). Numerical simulation of heat transfer and fluid flow over two rotating circular cylinders at low Reynolds number. *Heat Transfer-Asian Research*, 39(4), 246-261.
- Moshkin, N. P., & Suwannasri, P. (2010). Self-propelled motion of a torus rotating about its centerline in a viscous incompressible fluid. *Physics of Fluids*, 22(11), 113602.
- Moshkin, N. P., Sompong, J., & Suwannasri, P. (2013). Numerical study of flow and heat transfer from a torus placed in a uniform flow. *Journal of Engineering Thermophysics*, 22(2), 122-133.
- Roache, P. J. (1994). Perspective: A method for uniform reporting of grid refinement studies. *Journal of Fluids Engineering*, 116(3), 405-413.
- Sheard, G. J., Hourigan K., & Thompson, M. C. (2005). Computations of the drag coefficients for low-Reynolds-number flow past rings. *Journal of Fluid Mechanics*, 526, 257-275.
- Sheard, G. J., Thompson M. C., & Hourigan, K. (2003). From sphere to circular cylinders: the stability and flow structures of buff ring wakes. *Journal of Fluid Mechanics*, 492, 147-180.
- Soares, A. A., Ferreira, J. M., & Chhabra, R. P. (2005). Flow and forced convection heat transfer in crossflow of non-newtonian fluid over a circular cylinder. *Industrial and Engineering Chemistry Research*, 44(15), 5815-5827.
- Sungnul, S., & Moshkin, N. P. (2006). Numerical simulation of steady viscous flow past two rotating circular cylinders. *Suranaree Journal of Science and Technology*, 13(3), 219-233.
- Suwannasri, P. (2010). Characteristics of axisymmetric viscous in compressible flow passing a torus rotating about its centerline. *Songklanakalin Journal of Science and Technology*, 38(3), 319-324.
- Yanenko, N. N. (1971). *The method of Fractional Steps*. Berlin, Germany: Springer.